SIMULATION OF GRAVITY WAVE FIELDS AND THEIR EFFECTS ON THE LARGE-SCALE FLOW IN THE MARTIAN ATMOSPHERE USING A HIGH-RESOLUTION GENERAL CIRCULATION MODEL

T. Kuroda, *National Institute of Information and Communications Technology, Koganei, Tokyo, Japan (tkuroda@nict.go.jp),* **A.S. Medvedev, P. Hartogh**, *Max Planck Institute for Solar System Research, Göttingen, Germany*, **E. Yiğit**, *Department of Physics and Astronomy, George Mason University, Fairfax, VA, USA.*

Introduction:

Gravity waves (GWs) are small-scale atmospheric waves generated by various geophysical processes, such as topography, convection, and dynamical instability. On Mars, with much rougher topography than on Earth, strong convection and volatile instabilities of weather systems, GWs have larger amplitudes than on Earth. Observations [e.g. Creasey et al., 2006a; Fritts et al., 2006] and simulations [Medvedev et al., 2011a] have revealed that GWs strongly affect temperature and wind fields in the middle and upper atmosphere. Accurate estimate of GW activity in the lower atmosphere is important for constraining GW parameterizations and, as a result, for capturing effects of waves in the middle and upper atmosphere.

Our previous study using the Max Planck Institute Martian General Circulation Model (MPI-MGCM) and the nonlinear spectral whole atmosphere parameterization of small-scale GWs by Yiğit et al. [2008] have shown that the dynamical forcing of GWs significantly change the winds, reversing its direction above ~100 km [Medvedev et al., 2011a]. We also have shown that the thermal effects induced by GWs can be the main source of cooling above ~120 km, reproducing the observed temperature structure on Mars [Medvedev and Yiğit, 2012]. Similar physical importance of GWs has previously been demonstrated for the general circulation of Earth's upper atmosphere using the whole atmosphere parameterization [Yiğit et al., 2009, 2012; Yiğit and Medvedev, 2009]. Because of the lack of observations of small-scale fields on Mars, the global picture of GW activity is yet to be revealed. Therefore, we apply a high-resolution (GW-resolving) MGCM to provide a surrogate for observations with the goal of constraining GW parameterizations and validating their applications in MGCMs with a conventional (low) resolution.

In order to investigate the global distribution of small-scale GWs in the Martian atmosphere, we have conducted the first simulations with a high-resolution MGCM, using the DRAMATIC (Dynamics, RAdiation, MAterial Transport and their mutual InteraCtions) MGCM [Kuroda et al., 2015, 2016].

Model Description:

The MGCM was run at the T106 spectral truncation, which corresponds approximately to a 1.1°× 1.1° (or ~67 km) horizontal resolution. In the vertical direction, the model domain extends from the surface to ~80–100 km and is represented by 49 sigma-levels. Such setup allows for realistically capturing generation and propagation of GWs with horizontal wavelengths of ~200 km and longer and, to some extent, their vertical attenuation due to nonlinear processes. The MGCM utilizes the LTE radiation scheme for CO_2 molecules based on the correlated k-distribution method which accounts for the radiative transfer in infrared (including the 15 μm band) and near-infrared. Thus, effects of CO_2 cooling on the large-scale flow and small-scale disturbances have been accounted in the MGCM self-consistently. Note also that no GW parameterization is included in the model.

Results:

We considered horizontal-scale fluctuations with a total wave number s of larger than 60 (horizontal wavelengths of less than ~350 km) as GW-induced disturbances. The effects of the disturbances with smaller total wavenumbers ($21 \leq s \leq 30$ and $31 \leq s \leq 60$, which correspond to the wavelengths of 700-1050 km and 350-700 km, respectively) are also discussed for comparison.

Features in the northern hemisphere winter

Figure 1 shows the spatial distributions of the kinetic (E_k) and potential (E_p) energies averaged in 10-30 km, and their ratio (E_k/E_p), associated with GW activity in the northern winter solstice. The model reveals a latitudinal asymmetry with stronger wave activity in the winter hemisphere, and the simulated E_p distribution induced by GWs is in a good agreement with the available radio occultation data [Creasey et al., 2006]. The distribution of E_k/E_p shows that GWs are generated in the winter polar jet in northern hemisphere (where E_k/E_p is large), and mountain regions in southern hemisphere (where E_k/E_p is small). The zonal and meridional momentum flux distributions in the lower (260 Pa, ~10 km height) atmosphere are shown in Figure 2. In low latitudes, sources are localized both in space and time. In the northern middle- and high-latitudes, the distribution of the zonal flux is smooth, associated with the winter westerly jet and Kelvin waves (see also the Movie S1 of Kuroda et al. [2015]).

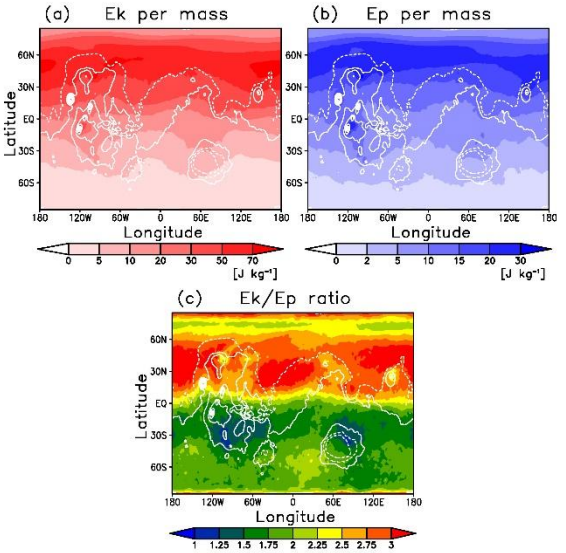

Figure 1: Simulated (a) E_k and (b) E_p (in J kg^{-1}) of resolved GWs with the total wave numbers of >60 (wavelengths of <~350 km), and (c) the ratio E_k/E_p, averaged between 10 and 100 Pa (10-30 km height) for 20 sols around L_s = 270°. White contours on each plot denote the Martian topography. After Kuroda et al. [2015].

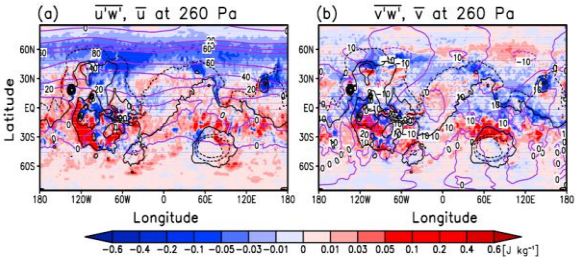

Figure 2: Color shades represent the distributions of horizontal fluxes of (a) zonal and (b) meridional wave momentum at 260 Pa overlapped by the time-mean zonal and meridional wind velocities, respectively (purple contours), around L_s = 270°. Black contours denote the Martian topography. After Kuroda et al. [2015].

Figure 3 shows the wavenumber dependence in the GW energy (sum of E_k and E_p) sources in the lower (260 Pa, ~10 km height) atmosphere in northern winter. It is shown that *s*=61-106 GWs are generated predominantly in low-and middle-latitudes. Longer wavelength disturbances (*s*=21-30) are mainly generated in high-latitudes and mountain regions. *s*=31-60 disturbances are strong in the southern hemisphere (around sub-solar latitudes).

Figure 4 shows the same as Figure 3, except in the upper atmosphere (0.1 Pa, ~80 km height). Orographic GWs are attenuated or filtered upon propagating upward, and the mesosphere is dominated by waves with faster horizontal phase velocities. Distributions of the ratios of GW wavelengths become mostly uniform for all components (spatial differences of less than ~10%). High GW energy is seen in winter polar regions, and 60-70% of the energy comes from the s=61-106 harmonics.

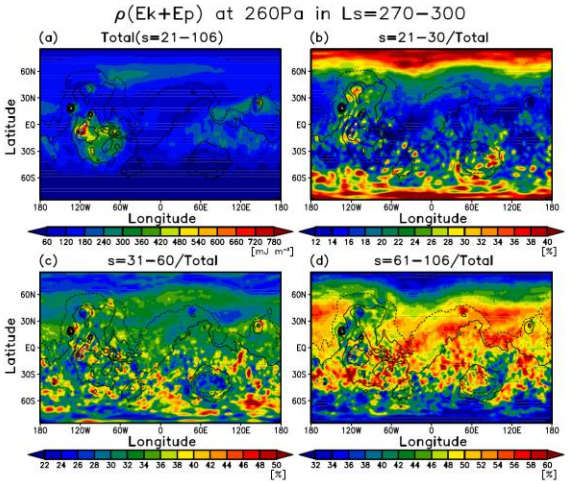

Figure 3: Longitude-latitude distribution of wave energy at 260 Pa pressure level averaged in L_s=270°-300°: (a) due to all disturbances with the horizontal wavenumber $s \geq 21$; (b) ratio (in per cent) of the energy due to s=21-30, (c) s=31-60 and (d) s=61-106 harmonics, respectively. Black contours denote the Martian topography. After Kuroda et al. [2016].

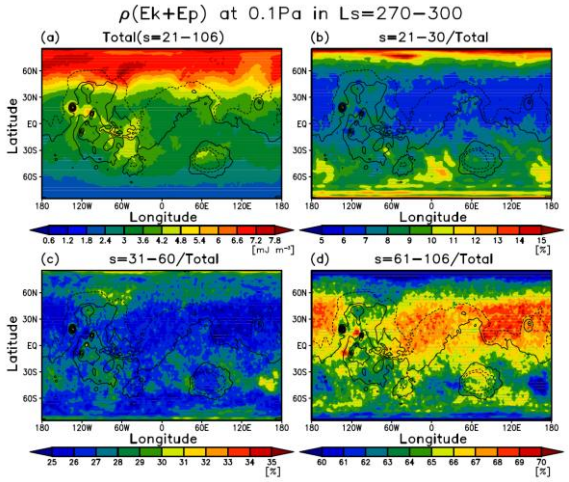

Figure 4: Same as Figure 3, except at 0.1 Pa pressure level. After Kuroda et al. [2016].

Wave fluxes are directed mainly against the local wind, with a clear relation between wave dissipation (divergence of the fluxes) and larger-scale wind acceleration. Figure 5 shows the acceleration rates of zonal and meridional wind velocities due to GWs simulated in this model. Effects of horizontal propagation on the acceleration are much smaller than those of vertical propagation (except the meridional acceleration rates in high latitudes). Also, the values are comparable to those obtained from the whole atmosphere nonlinear GW drag parameterization [Yiğit et al., 2008; Medvedev et al., 2011a, 2011b].

Figure 6 shows the temperature and wind fields in comparison with our low horizontal resolution of T21 (5.6°× 5.6°, or ~333 km) simulation. It is shown that resolved GWs in the T106 simulation enhances

the meridional circulation, which results in the stronger winter polar warming, and weaken the zonal jets in both hemispheres as parameterized in the work by Medvedev et al. [2011a].

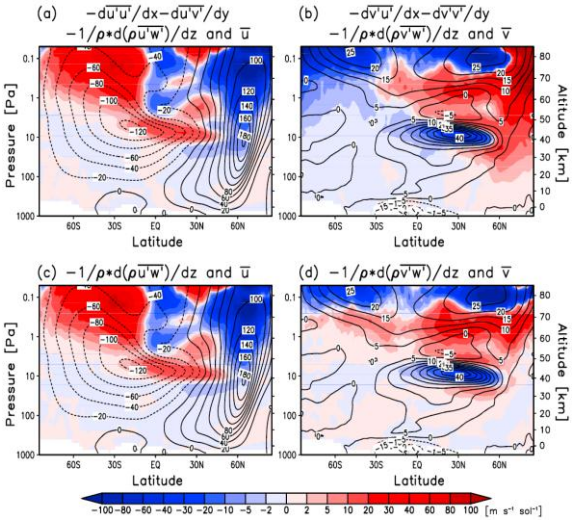

Figure 5: Divergences of gravity wave momentum fluxes (shaded, in m s^{-1} sol^{-1}) and the mean wind (contours, in m s^{-1}) around L_s = 270°: full (horizontal and vertical) divergences of (a) zonal and (b) meridional momentum fluxes, only vertical divergences of (c) zonal and (d) meridional momentum fluxes. After Kuroda et al. [2015].

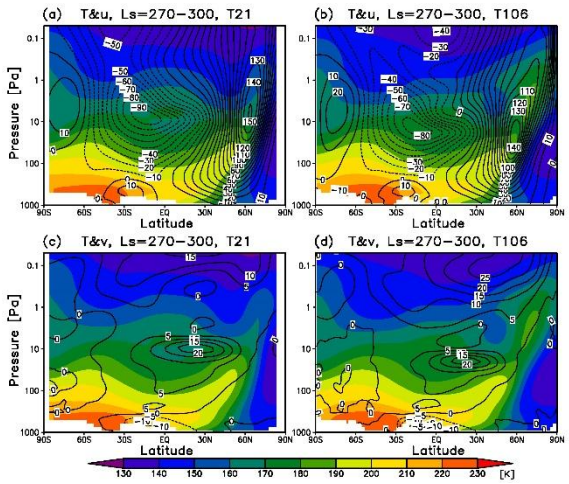

Figure 6: (a) Zonal-mean temperature (K, shaded) and zonal wind velocity (m s^{-1}, contours) averaged in L_s=270°-300° simulated by our MGCM with the horizontal resolution of T21. (b) Same as (a) except the horizontal resolution of T106. (c) and (d) are the same as (a) and (b), respectively, except that the contours represent zonal-mean meridional wind velocity (m s^{-1}).

Seasonal change.

We have extended the T106 simulation into a whole year. Figure 7 shows the seasonal changes of zonal-mean E_k, E_k/E_p and zonal momentum flux at 260 Pa. As seen from the results of E_k, generations of GWs in low-latitudes are much stronger in northern winter (around the perihelion) than in northern summer (around the aphelion). In mid-latitudes of both hemispheres during winter, the negative zonal momentum flux appears along with the westerly wind fields, as well as small E_k/E_p, which shows that the GWs are generated in the westerly polar jets in all seasons.

Figure 8 shows the seasonal changes of zonal momentum flux and wind acceleration rates. These values are clearly associated with the seasonal changes of mean background wind fields, which shows that overall the GWs significantly decelerate the wind velocity in all seasons.

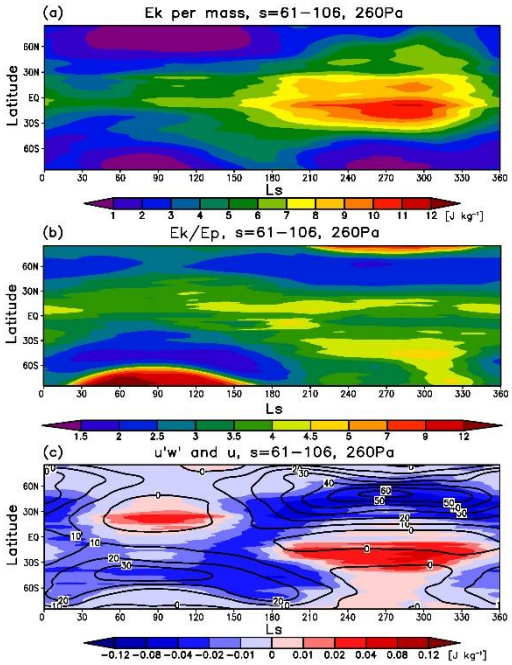

Figure 7: L_s (season)-latitude cross sections of zonal-mean (a) E_k, (b) E_k/E_p and (c) zonal momentum flux at 260 Pa pressure level

Summary:

We performed simulations with the high-resolution (T106) DRAMATIC MGCM to directly investigate generation and propagation of GWs with horizontal scales of *s*=61-106 (200-350 km wavelength) from their sources in the lower atmosphere to the mesosphere. The zonal-mean temperature and wind fields in a high-resolution simulation are significantly affected by the resolved GWs, in comparison with the results by a low-resolution (T21) simulation. This approach provides a direct validation for results obtained previously with parameterized GW effects.

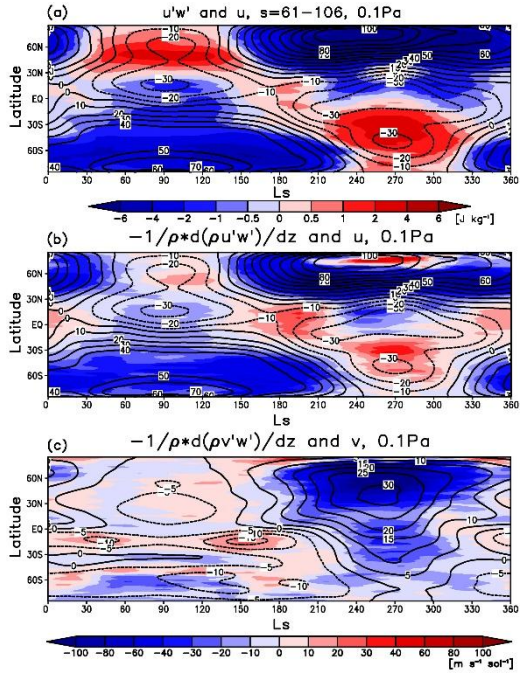

Figure 8: L_s-latitude cross sections of zonal-mean (a) zonal momentum flux, and vertical divergences of (b) zonal and (c) meridional momentum fluxes at 260 Pa pressure level.

In the northern winter, our simulations show that there are two main sources of GWs: mountainous regions and the meandering winter polar jet. In comparison with the longer-scale (s=21-30 and s=31-60) harmonics, generations of the shorter-scale GWs (s=61-106) are distinctive in the low-latitudes, and the shorter-scale harmonics progressively dominate with height. Orographic GWs are filtered or significantly dissipated upon propagating upward, and the mesosphere is primarily dominated by waves with faster horizontal phase velocities. Wave fluxes are directed mainly against the local wind, with a clear relation between wave dissipation and wind acceleration. GW dissipation in the upper mesosphere generates a body force per unit mass of tens of m s^{-1} per Martian solar day (sol^{-1}), which tends to close the simulated jets. Effects of horizontal propagation of GWs on the acceleration are much smaller than those of vertical propagation, and the results of acceleration rates are comparable to those obtained from the application of the whole atmosphere GW parameterization by Yiğit et al. [2008], which considers only the vertical propagations of a broad spectrum of small-scale GWs.

The results represent a realistic surrogate for missing observations, which can be used to further constrain GW parameterizations and validate GCMs. Observations of GWs in the thermosphere by the MAVEN mission [e.g., Yiğit et al. 2015], and further modeling of GW propagation into the thermosphere by the MPI-MGCM in the light of our modeling study would provide deeper insight into the global distribution of GW activity and the associated effects on Mars.

References:

Creasey, J.E. et al., 2006: Global and seasonal distribution of gravity wave activity in Mars' lower atmosphere derived from MGS radio occultation data. *Geophys. Res. Lett.*, **33**, L01803, doi:10.1029/2005GL024037.

Fritts, D.C. et al., 2006: Mean and gravity wave structures and variability in the Mars upper atmosphere inferred from Mars Global Surveyor and Mars Odyssey aerobraking densities. *J. Geophys. Res.*, **111**, A12304, doi:10.1029/ 2006JA011897.

Kuroda, T. et al., 2015: A global view of gravity waves in the Martian atmosphere inferred from a high-resolution general circulation model. *Geophys. Res. Lett.*, **42**, 9213–9222, doi:10.1002/2015GL066332.

Kuroda, T. et al., 2016: Global distribution of gravity wave sources and fields in the Martian atmosphere during equinox and solstice inferred from a high-resolution general circulation model. *J. Atmos. Sci..*, in press, doi: 10.1175/JAS-D-16-0142.1.

Medvedev, A.S. et al., 2011a: Influence of gravity waves on the Martian atmosphere: General circulation modeling. *J. Geophys. Res.*, **116**, E10004, doi:10.1029/ 2011JE003848.

Medvedev, A.S. et al., 2011b: Estimates of gravity wave drag on Mars: Indication of a possible lower thermosphere wind reversal. *Icarus*, **211**, 909–912, doi:10.1016/ j.icarus.2010.10.013.

Medvedev, A.S. and E. Yiğit, 2012: Thermal effects of internal gravity waves in the Martian upper atmosphere. *Geophys. Res. Lett.*, **39**, L05201, doi:10.1029/2012GL 050852.

Yiğit, E. et al., 2008: Parameterization of the effects of vertically propagating gravity waves for thermosphere general circulation models: Sensitivity study. *J. Geophys. Res.*, **113**, D19106, doi:10.1029/2008JD010135.

Yiğit, E. et al., 2009: Modeling the effects of gravity wave momentum deposition on the general circulation above the turbopause. *J. Geophys. Res.*, **114**, D07101, doi:10.1029/ 2008JD011132.

Yiğit, E. and A. S. Medvedev, 2009: Heating and cooling of the thermosphere by internal gravity waves. *Geophys. Res. Lett.*, **36**, L14807, doi:10.1029/2009GL 038507.

Yiğit, E. et al., 2012: Dynamical effects of internal gravity waves in the equinoctial thermosphere, *J. Atmos. Sol.-Terr. Phys.*, **90-91**, 104–116.

Yiğit, E. et al., 2015: High-altitude gravity waves in the Martian thermosphere observed by MAVEN/NGIMS and modeled by a gravity wave scheme, *Geophys. Res. Lett.*, **42**, doi:0.1002/2015GL065307.